Second International Conference on
Fuel Cell Science, Engineering and Technology

FuelCell2004 – xxxx

INFLUENCE OF POROUS ELECTRODE STRUCTURE ON PEM FUEL CELLS DESIGN AND PERFORMANCE

Pietro Asinari[1] – Marco Coppo[2]

Dipartimento di Energetica, Politecnico di Torino, Turin, Italy
[1]Email: pietro.asinari@polito.it
[2]Email: marco.coppo@polito.it

ABSTRACT

Gas flow in fuel cell porous electrodes is usually modelled with Darcy's law, which requires the definition of a resistance constant for the material. This can be done directly via experimentation or indirectly via numerical tuning to fit experimental data on cell behaviour. Both methods lack generality, as they do not take into account the particular porous structure of each electrode.

In the present work, a numerical procedure for calculating the resistance constant for a given porous structure is presented. This procedure is based on Lattice Boltzmann models, which treat the problem from a microscopic point of view, reproducing collisions between fluid molecules and solid particles. It can be demonstrated that under certain hypotheses, these models yield Navier-Stokes equations on a macroscopic scale, hence obeying fluid mechanics laws.

Here the flow in a set of thirty randomly generated porous structures was analyzed, thus obtaining a distribution of values for Darcy's constant. The analysis was repeated for ten different pressure gradients applied to a portion of the electrode and for three different volume porosities.

The results showed that, for a given volume porosity, the value of Darcy's constant is strongly affected by the material porous structure. On the other hand, the mean value of resistance remained almost constant while varying the applied load, thus correctly reproducing the linear dependence between velocity and pressure gradient, as stated by Darcy's law.

As fuel cell models are a great help in designing and predicting component operation, a further analysis was carried out in order to study the influence of the electrode resistance constant on cell performance prediction. The Lattice Boltzmann model was used to obtain resistance data characteristic of fuel cell electrodes, and the results were implemented in a one dimensional fuel cell model.

The simulations showed that the variation of Darcy's constant does not significantly affect the prediction of the cell polarization curve, while a significant effect was found on the prediction of the exact operating point on the polarization curve.

In conclusion, if accurate modelling of a fuel cell is required, great care must be taken in evaluating the electrodes resistance constant. The procedure presented here, coupled with a non destructive tomography scan of the electrode structure could greatly help in refining existent fuel cell models.

INTRODUCTION

Throughout the last decade, a considerable amount of work was carried out in order to obtain ever more refined models of proton exchange membrane (PEM) fuel cells. The mathematical models obtained were first numerically implemented in one dimension [1-6] whereas, recently, several research groups have produced detailed three-dimensional models of this type of fuel cell [7-15]. Such models helped considerably in understanding the complex phenomena occurring during fuel cell operation, thus allowing a more accurate cell design.

While the refinement of modelling techniques and the increase in computer power allowed for the creation of very accurate fuel cell numerical models, the developers of such tools always faced the same problem: retrieving reliable physical data concerning fuel cells parts. The lack of accuracy and reliability of numerical constants used in the models seriously affects, and in some cases cancels out, the improvements done in the numerical code. Post process tuning of physical parameters to fit model predictions with experimental data is the way normally followed in this case. This problem is of particular significance when dealing with fuel cell models, as the experimental data available is usually limited to the cell polarization curve, which represents the integral of the effects of all the constants used in the model.

Flow of gases in fuel cell porous electrodes is usually modelled with Darcy's law. This characterizes the material with a resistance constant, to be evaluated experimentally or numerically adjusted to match experimental data. Both these methods pose problems when dealing with fuel cells. The small electrode thickness makes it difficult to accurately measure the material hydraulic constant and guarantee its independence from the electrode porous structure. On the other hand, the numerical tuning of such a parameter to fit experimental data of cell performance, namely its polarization curve, neither guarantees that the true value is found, as the cell behaviour also depends on other adjustable parameters, nor its independence from the different load conditions.

The present study tries to address the problem following an alternative approach. Here a procedure for calculating the hydraulic constant as a function of material structure and applied pressure gradient was defined. Even though common numerical codes for a Navier-Stokes model could be used to solve the flow in each microchannel of the porous media, computational overhead and heavy post-processing render them unsuitable for solving the flow in the porous material and obtaining Darcy's constant.

On the other hand, the lattice Boltzmann methods (LBMs) are efficient numerical tools to investigate flows in highly complex geometries, such as porous media [16, 17, 18]. Even though traditional Navier-Stokes solvers could be used to describe porous media flow, LB methods do not require pressure-velocity decoupling or the resolution of a large system of algebraic equations [19, 20]. They solve a simplified Boltzmann equation for an ensemble-averaged distribution of moving, interacting particles on a discrete lattice. The macroscopic quantities that describe the fluid flow can be calculated as integrals of this distribution. Since the motion of particles is limited to fixed paths connecting lattice nodes, the resolution process needs only information about nearest neighbour nodes. In this way, fluid flow through complex geometry can be analyzed by means of an easier mesoscopic approach. Analogous considerations apply to wall boundary conditions, such as those in porous media. They can be easily implemented for any geometric configuration in order to ensure no-slip condition at solid occlusions.

The aim of the present paper is twofold. Firstly, to investigate the influence of different porous structures on the material resistance constant in order to evaluate whether different structures with the same volume porosity behave differently with respect to fluid flow through them. Secondly, to evaluate in which way different electrode porous structures, characterized by the same value of volume porosity, affect the prediction of fuel cell operation by a one-dimensional numerical model.

MATHEMATICAL MODEL FOR POROUS MEDIA FLOW

Continuous model

Under some simplifying hypotheses, kinetic theory states that the evolution of the single particle density distribution in a rarefied gas of rigid spheres obeys the Boltzmann equation [21].

$$\frac{\partial f}{\partial t} + \mathbf{v}\cdot\nabla f + \mathbf{a}\cdot\nabla_{\mathbf{v}} f = Q(f, f) \tag{1}$$

where $f(\mathbf{x},\mathbf{v},t)$ is the continuous single particle distribution function, $\mathbf{v}$ is the microscopic velocity, $\mathbf{a}$ is the acceleration due to an external field, and the quadratic expression $Q(f, f)$ is the collision integral. Macroscopic quantities, such as the density $\rho(\mathbf{x}, t)$ and the macroscopic velocity $\mathbf{u}(\mathbf{x}, t)$, can be calculated as the moments of the density distribution function:

$$\rho(\mathbf{x}, t) = \int_{-\infty}^{+\infty} m f \prod_{k=1}^{D} dv_k \tag{2}$$

$$\rho(\mathbf{x}, t)\,\mathbf{u}(\mathbf{x}, t) = \int_{-\infty}^{+\infty} m\,\mathbf{v}\, f \prod_{k=1}^{D} dv_k \tag{3}$$

The collision integral $Q(f, f)$ in the Boltzmann equation can be replaced by the single-relaxation-time collision model $J(f)$ proposed originally by Bhatnagar, Gross, and Krook (BGK) [22].

$$\frac{\partial f}{\partial t} + \mathbf{v}\cdot\nabla f + \mathbf{a}\cdot\nabla_{\mathbf{v}} f = J(f) = -\frac{1}{\tau}(f - f^e) \tag{4}$$

where τ is the relaxation time and f^e is the Maxwellian equilibrium distribution function which gives a vanishing collision integral $Q(f^e, f^e) = 0$, i.e.

$$f^e(\mathbf{x}, \mathbf{v}, t) = \frac{\rho}{m}\left(\frac{3}{2\pi c^2}\right)^{D/2} \exp\left[-\frac{3}{2}\frac{(\mathbf{v}-\mathbf{u})^2}{c^2}\right] \tag{5}$$

where $c(\mathbf{x}, t)$ is a scalar characteristic velocity which can be expressed physically in terms of internal energy.

The term that takes into account the effect of the external force field can be simplified as follows [23]:

$$\nabla_{\mathbf{v}} f \cong \nabla_{\mathbf{v}} f^e = -\frac{3}{c^2} f^e (\mathbf{v}-\mathbf{u}) \tag{6}$$

Substituting equation (6) into equation (4) yields the final form of the adopted BGK model.

$$\frac{\partial f}{\partial t} + \mathbf{v}\cdot\nabla f = -\frac{1}{\tau}(f - f^e) + \frac{3}{c^2} f^e (\mathbf{v}-\mathbf{u})\cdot\mathbf{a} \tag{7}$$

Using the Chapman-Enskog procedure, a suitable expansion of certain solutions of equation (7) recovers the Navier-Stokes macroscopic description when the bulk viscosity is neglected [23]. Thus,

$$\frac{\partial \rho}{\partial t} + \nabla\cdot(\rho\mathbf{u}) = 0 \tag{8}$$

$$\begin{aligned}\frac{\partial}{\partial t}(\rho\mathbf{u}) + \nabla\cdot(\rho\,\mathbf{u}\otimes\mathbf{u}) = \\ -\nabla p + \nabla\cdot\left[\rho\zeta(\nabla\mathbf{u} + \nabla\mathbf{u}^T)\right] + \rho\,\mathbf{a}\end{aligned} \tag{9}$$

where $p = \rho c^2/3$ can be identified with the pressure and $\zeta = \tau c^2/3$ with the cinematic viscosity of the fluid. A proper set of boundary conditions for single particle distribution function must be considered in order to ensure the no-slip condition at the walls.

Discrete model

To solve the BGK equation (7), the discrete ordinate method can be applied [24]. According to this method, a set of discrete microscopic velocities $\mathbf{v}_i$ must be defined on which the distribution function is evaluated. The generic function $f_i(\mathbf{x}, t)$ is the single particle distribution function evaluated for velocity $\mathbf{v}_i$ at $(\mathbf{x}, t)$. Hence the BGK equation, which is an integro-differential equation, reduces to a system of differential equations, such that

$$\frac{\partial f_i}{\partial t} + \mathbf{v}_i\cdot\nabla f_i = -\frac{1}{\tau}(f_i - f_i^e) + \frac{3}{c^2} f_i^e (\mathbf{v}_i - \mathbf{u})\cdot\mathbf{a} \tag{10}$$

Since only the distribution functions for discrete microscopic velocities are considered, an interpolation test function must be adopted to calculate the macroscopic quantities. In this way, the previous integrals (equations (2) and (3)) reduce to weighted summations of the considered functions. The interpolation test function should be as similar to the Maxwellian distribution function as possible in order to easily include the equilibrium conditions. If we consider the regime of low speed fluid motion $|\mathbf{u}| << |\mathbf{v}|$, the equilibrium distribution function

(equation (5)) can be linearised around the state at rest [24], namely,

$$f^e(\mathbf{x},\mathbf{v},t) \cong K(\mathbf{v})\,\varphi^e(\mathbf{x},\mathbf{v},t) \tag{11}$$

where

$$K(\mathbf{v}) = \frac{1}{m\,c^D}\left(\frac{3}{2\pi}\right)^{D/2} \exp\left(-\frac{3}{2}\frac{\mathbf{v}\cdot\mathbf{v}}{c^2}\right) \tag{12}$$

$$\varphi^e(\mathbf{x},\mathbf{v},t) = \rho\left[1+3\frac{\mathbf{v}\cdot\mathbf{u}}{c^2}+\frac{9}{2}\left(\frac{\mathbf{v}\cdot\mathbf{u}}{c^2}\right)^2-\frac{3}{2}\frac{\mathbf{u}\cdot\mathbf{u}}{c^2}\right] \tag{13}$$

Since the deviation of the distribution function from the one at rest is also small, it is assumed that the function $\varphi(\mathbf{x},\mathbf{v},t) = f(\mathbf{x},\mathbf{v},t)/K(\mathbf{v})$ can be approximated by an interpolation test function $\tilde{\varphi}(\mathbf{x},\mathbf{v},t) = \tilde{f}(\mathbf{x},\mathbf{v},t)/K(\mathbf{v})$, which is a D dimensional polynomial of second degree as it rigorously happens for the function $\varphi^e(\mathbf{x},\mathbf{v},t)$. This test function includes $1+2D$ unknown parameters, which can be determined by using the values of the distribution function for discrete microscopic velocities $\tilde{\varphi}(\mathbf{x},\mathbf{v}_i,t) = f_i(\mathbf{x},t)/K(\mathbf{v}_i) = \varphi_i(\mathbf{x},t)$. The modified distributions functions for discrete microscopic velocities $\varphi_i(\mathbf{x},t)$ satisfy a system of differential equations similar to the original one (equation (10)) for $f_i(\mathbf{x},t)$.

The macroscopic quantities operative definitions must be modified according to the discrete ordinate method [24]. Thus,

$$\tilde{\rho}(\mathbf{x},t) = \int_{-\infty}^{+\infty} m\,\tilde{f}\prod_{k=1}^{D} dv_k = \sum_{i=1}^{Q} W_i\, f_i = \sum_{i=1}^{Q} w_i\,\varphi_i \tag{14}$$

$$\tilde{\rho}(\mathbf{x},t)\,\tilde{\mathbf{u}}(\mathbf{x},t) = \int_{-\infty}^{+\infty} m\,\mathbf{v}\,\tilde{f}\prod_{k=1}^{D} dv_k = \sum_{i=1}^{Q} W_i'\, f_i\,\mathbf{v}_i = \sum_{i=1}^{Q} w_i'\,\varphi_i\,\mathbf{v}_i \tag{15}$$

where W_i, W_i', w_i and w_i' are the dimensionless coefficients of the quadratures. Since usually the number of unknowns for the interpolation test function, *1+2D*, is smaller than the number of discrete microscopic velocities, *Q*, the problem is ill posed and a proper strategy must be adopted in order to recover the Navier-Stokes macroscopic equations.

The system of differential equations for modified distribution functions can be simplified by applying the method of characteristics. Let us consider the sheaf of characteristic surfaces for each discrete microscopic velocity.

$$\mathbf{x}_i(t) = \int_0^t \mathbf{v}_i\,dt + \alpha_i \tag{16}$$

Moving on characteristic surfaces, the rate of change for the distribution function reduces to a time function, and our system of differential equations becomes:

$$\frac{\partial\varphi_i}{\partial t} + \mathbf{v}_i\cdot\nabla\varphi_i = \frac{\partial\varphi_i}{\partial t} + \frac{\partial\mathbf{x}}{\partial t}\cdot\nabla\varphi_i = \frac{d}{dt}\varphi_i(\mathbf{x}_i,t) = -\frac{1}{\tau}(\varphi_i-\varphi_i^e) + \frac{3}{c^2}\varphi_i^e\,(\mathbf{v}_i-\mathbf{u})\cdot\mathbf{a} \tag{17}$$

Finally, the explicit Euler rule can be applied, such that

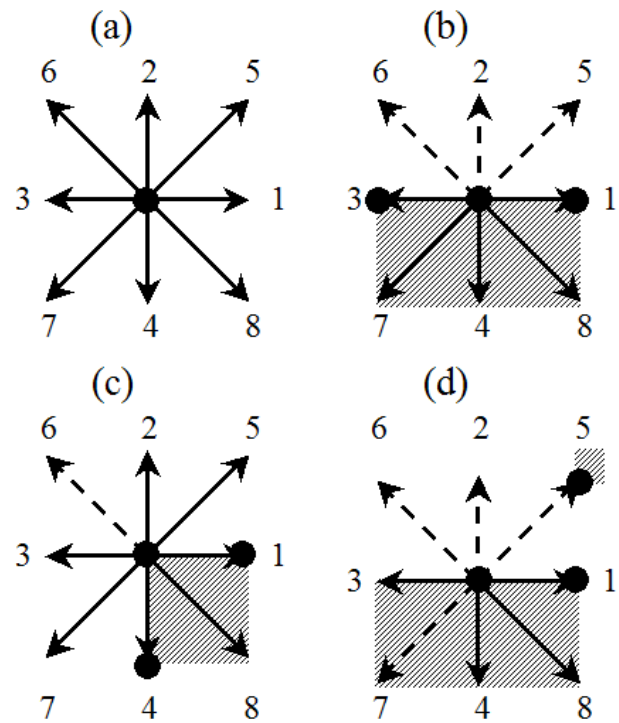

Fig. 1: Lattice discrete velocities for D2Q9.

$$\varphi_i(\mathbf{x}+\mathbf{v}_i\,\delta t, t+\delta t) = \left(1-\frac{\delta t}{\tau}\right)\varphi_i(\mathbf{x},t) + \frac{\delta t}{\tau}\varphi_i^e(\mathbf{x},t) + \frac{3\,\delta t}{c^2}\varphi_i^e\,(\mathbf{v}_i-\mathbf{u})\cdot\mathbf{a} \tag{18}$$

where δt is the time step, which must satisfy the stability threshold $\delta t < 2\tau$.

In the following computations, a square lattice ($D2Q9$) [25] which makes use of a two-dimensional computational domain ($D=2$) and nine discrete velocities ($Q=9$) is considered. The lattice discrete velocities are shown in Figure 1a and are analytically given by:

$$\mathbf{v}_i = \begin{cases} i=0 \qquad [0,0] \\ i=1,2,3,4 \\ \qquad c\,[\cos(i\pi/2-\pi/2), \sin(i\pi/2-\pi/2)] \\ i=5,6,7,8 \\ \qquad c\sqrt{2}\,[\cos(i\pi/2-9\pi/4), \sin(i\pi/2-9\pi/4)] \end{cases} \tag{19}$$

In this case, a proper strategy for the choice of the dimensionless coefficients of the quadratures is: $w_0 = w'_0 = 4/9$, $w_i = w'_i = 1/9$ for $i=1,2,3,4$ and $w_i = w'_i = 1/36$ for $i=5,6,7,8$. These values allow satisfying the operative definitions of macroscopic quantities, equations (14) and (15).

Let us consider the following equivalence for the considered lattice:

$$\sum_{i=1}^{Q} w_i\,\mathbf{v}_i\otimes\left[\varphi_i^e\,(\mathbf{v}_i-\mathbf{u})\right] = \sum_{i=1}^{Q} w_i\,\mathbf{v}_i\otimes\left(\frac{\rho}{18\,w_i}\mathbf{v}_i\right) \tag{20}$$

Since the effect of the external force field appears only in the momentum equation (9), the previous equivalence can be used to simplify the discrete BGK equation (18) [26], which becomes

$$\varphi_i(\mathbf{x}+\mathbf{v}_i\,\delta t, t+\delta t) = \left(1-\frac{\delta t}{\tau}\right)\varphi_i(\mathbf{x},t) + \frac{\delta t}{\tau}\varphi_i^e(\mathbf{x},t) + \frac{\delta t}{6\,w_i\,c^2}\mathbf{v}_i\cdot\mathbf{g} \tag{21}$$

where $\mathbf{g} = \rho\,\mathbf{a}$.

A Chapman-Enskog procedure is again applied to derive the macroscopic equations of the model, namely,

$$\frac{\partial\tilde{\rho}}{\partial t} + \nabla\cdot(\tilde{\rho}\,\tilde{\mathbf{u}}) = 0 \tag{22}$$

$$\frac{\partial}{\partial t}(\tilde{\rho}\tilde{\mathbf{u}}) + \nabla\cdot(\tilde{\rho}\,\tilde{\mathbf{u}}\otimes\tilde{\mathbf{u}}) = -\nabla\left(\frac{c^2}{3}\tilde{\rho}\right) + \nabla\cdot\left[\tilde{\zeta}\,\nabla(\tilde{\rho}\,\tilde{\mathbf{u}}) + \tilde{\zeta}\,\nabla(\tilde{\rho}\,\tilde{\mathbf{u}})^T\right] + \mathbf{g} \tag{23}$$

where $\tilde{\zeta} = \zeta\,(1-0.5\,\delta t/\tau)$. The previous equations are valid only if the low speed limit $|\mathbf{u}| << c$ is satisfied, as highlighted in the derivation process. The macroscopic equations for the discrete model (22, 23) do not recover directly the Navier-Stokes model, as it happened for the continuous model (8, 9). Some hypotheses must be introduced to eliminate this discrepancy.

Electrode model

The discrepancy with the Navier-Stokes model resides in the momentum equation, given by

$$\frac{\partial}{\partial t}(\tilde{\rho}\tilde{\mathbf{u}}) + \nabla\cdot(\tilde{\rho}\,\tilde{\mathbf{u}}\otimes\tilde{\mathbf{u}}) = -\nabla\left(\frac{c^2}{3}\tilde{\rho}\right) + \nabla\cdot\left[\tilde{\rho}\,\tilde{\zeta}\,(\nabla\tilde{\mathbf{u}} + \nabla\tilde{\mathbf{u}}^T)\right] + \mathbf{g} + \mathbf{e} \tag{24}$$

where

$$\mathbf{e} = \nabla\cdot\left(\tilde{\zeta}\;\tilde{\mathbf{u}}\otimes\nabla\tilde{\rho} + \tilde{\zeta}\;\nabla\tilde{\rho}\otimes\tilde{\mathbf{u}}\right) \tag{25}$$

If the compressibility factor is small enough, then the density gradients are mainly due to pressure gradients $\nabla\tilde{\rho} = \nabla\tilde{p}/c_s^2$, where c_s is the speed of sound. If we consider the incompressible limit $|\mathbf{u}| << c_s$, the divergence argument in equation (25) is very small:

$$\left|\,\tilde{\zeta}\;\tilde{\mathbf{u}}\otimes\nabla\tilde{\rho} + \tilde{\zeta}\;\nabla\tilde{\rho}\otimes\tilde{\mathbf{u}}\,\right| << \left|\,\tilde{\rho}\;\tilde{\zeta}\;(\nabla\cdot\mathbf{u})\,\mathbf{I}\,\right| << 1 \tag{26}$$

If we suppose that the divergence argument does not change rapidly around zero, the error (equation (25)) can be neglected.

Let us consider a forcing term that depends on the pressure gradient $\mathbf{g} = -\beta\nabla\tilde{p}$. If the parameter β is properly chosen, i.e. $\beta = 1 - c^2/(3c_s^2)$, then the Navier-Stokes model is recovered, namely,

$$\frac{\partial}{\partial t}(\tilde{\rho}\tilde{\mathbf{u}}) + \nabla\cdot(\tilde{\rho}\,\tilde{\mathbf{u}}\otimes\tilde{\mathbf{u}}) = -\nabla\tilde{p} + \nabla\cdot\left[\tilde{\rho}\,\tilde{\zeta}\,(\nabla\tilde{\mathbf{u}} + \nabla\tilde{\mathbf{u}}^T)\right] \tag{27}$$

The previous equation is valid only if the low speed limit $|\mathbf{u}| << c$ (microscopic condition) and the incompressible limit $|\mathbf{u}| << c_s$ (macroscopic condition) are satisfied, as highlighted in the derivation process.

In the following computations, the lattice velocity c and the collision time τ are chosen in order to produce selected values for the cinematic viscosity ζ_0 and spatial step $\delta_0 = \delta x_0 = \delta y_0$. Thus,

$$c = \frac{6\,\omega}{2-\omega}\frac{\zeta_0}{\delta_0} \tag{28}$$

$$\tau = \frac{2-\omega}{6\,\omega^2}\frac{\delta_0^2}{\zeta_0} \tag{29}$$

where $\omega = \delta t/\tau$ is the dimensionless collision frequency and has a fixed value due to a stability criterion ($\omega = 1.2 \div 1.6$). The previous expressions (equations (28) and (29)) allow one to consider different spatial resolutions in order to produce a mesh-independent solution. In the following computations, a mesh-independent solution is found when the results for the default mesh and finer mesh differ by less than 2 %.

Finally, a proper set of boundary conditions must be considered [27, 28]. Since the computational domain was chosen to be smaller than the physical thickness of the electrode, periodic boundary conditions were considered at the domain border. Inside the domain, additional boundary conditions for single particle distribution functions must be considered in order to ensure the no-slip condition at the walls, i.e. at the interface with the solid occlusions. Let us consider the surface wall node shown in Figure 1b. The boundary is aligned with the x-direction and φ_2, φ_5, φ_6 are the inward-pointing links, which are unknown because they depend on the wall behaviour. The quadratures (equations (14) and(15)) and the specified velocity components $\tilde{u}_x = \tilde{u}_y = 0$ are not enough to determine φ_2, φ_5, φ_6 and $\tilde{\rho}$ because the resolution system is under determined. The additional condition needed is called the bounce-back rule and prescribes complete reflection for weighted inward-pointing distribution functions normal to the surface ($w_2\varphi_2$), namely

$$\begin{cases} w_2\varphi_2 + w_5\varphi_5 + w_6\varphi_6 - \tilde{\rho} = \\ \qquad - w_0\varphi_0 - w_1\varphi_1 - w_3\varphi_3 - w_4\varphi_4 - w_7\varphi_7 - w_8\varphi_8 \\ w_5\varphi_5 - w_6\varphi_6 = \tilde{\rho}\,\tilde{u}_x/c - w_1\varphi_1 - w_8\varphi_8 + w_3\varphi_3 + w_7\varphi_7 \\ w_2\varphi_2 + w_5\varphi_5 + w_6\varphi_6 = \tilde{\rho}\,\tilde{u}_y/c - w_7\varphi_7 - w_4\varphi_4 - w_8\varphi_8 \\ w_2\varphi_2 = w_4\varphi_4 \end{cases} \tag{30}$$

In this way, the problem is well posed and can be solved, resulting in

$$\begin{cases} \rho = w_0\varphi_0 + w_1\varphi_1 + w_3\varphi_3 + 2\,(w_4\varphi_4 + w_7\varphi_7 + w_8\varphi_8) \\ \varphi_5 = \left[w_7\varphi_7 - 0.5\,(w_1\varphi_1 - w_3\varphi_3)\right]/\,w_5 \\ \varphi_6 = \left[w_8\varphi_8 + 0.5\,(w_1\varphi_1 - w_3\varphi_3)\right]/\,w_6 \\ \varphi_2 = (w_4\varphi_4)/\,w_2 \end{cases} \tag{31}$$

Since the bounce-back method (BBM) was also applied originally to $w_5\varphi_5$ and $w_6\varphi_6$, the present one is called the improved bounce-back method, (IBBM) because it reduces the arbitrary assumptions [28]. It can be demonstrated that the IBBM is equivalent to supposing a preliminary distribution due to ideal reflection and then operating a mass redistribution for inward-pointing links. As evident from solutions (31), the IBBM allows one to determine the values of three unknown discrete distribution functions. When analyzing complex porous geometries, some configurations exist for which the number of unknown functions is smaller (see Figure 1c) or greater (see Figure 1d) than three. In the first case, the node is called over-conditioned, while in the second it is called under-conditioned. In both cases, the IBBM would produce ill-posed problems and it cannot be applied. In the

following computations, ill-posed configurations are analyzed by the original BBM.

Numerical implementation

A numerical code which implements the lattice Boltzmann scheme discussed in the previous sections was developed. A brief description of the main characteristics of the code is reported here.

In the following calculations, the collision operator in the discrete BGK equation (21) is assumed constant during each time step. This assumption introduces a second-order truncation error, but the only effect is a change of the effective viscosity ($\nu \rightarrow \tilde{\nu}$). The main advantage of this is the possibility to decouple the resolution of the BGK equation into two easier steps. During the collision step, the new discrete distribution functions are evaluated as follows

$$\varphi_i^*(\mathbf{x},t) = \left(1-\frac{\delta t}{\tau}\right)\varphi_i(\mathbf{x},t) + \frac{\delta t}{\tau}\varphi_i^e(\mathbf{x},t) + \frac{\delta t}{6\,w_i\,c^2}\mathbf{v}_i\cdot\mathbf{g} \tag{32}$$

During the streaming step, the new discrete distribution functions are properly assigned to correct spatial locations, i.e.

$$\varphi_i(\mathbf{x}+\mathbf{v}_i\,\delta t, t+\delta t) = \varphi_i^*(\mathbf{x},t) \tag{33}$$

At each time step, the operations performed by the code can be grouped into four phases:

1. ***Collision.*** The discrete Maxwellian equilibrium distribution functions are evaluated by using the macroscopic quantities and the new values for each discrete velocity are calculated by means of equations (32) and stored.
2. ***Streaming.*** The discrete distribution functions are updated according to equations (33).
3. ***Boundary conditions.*** All values of unknown discrete distribution functions for inward-pointing links are evaluated by BBM. For links that refer to nodes out of the computational domain, the periodic boundary conditions are directly applied. The subclass of inward-pointing links, which belong to well-posed configurations, are corrected according to IBBM so as to ensure the no-slip condition.
4. ***Moments.*** The macroscopic quantities, which are moments of the distribution function, are evaluated by means of equations (14, 15).

The main goal of the numerical code is to calculate the mass flow rate induced by a given pressure drop applied to a randomly generated porous structure, so as to evaluate the material resistance constant that appears in Darcy's law. Let us define a hydraulic parameter $k_D(\nabla p)$ as

$$\langle \rho\,\mathbf{u}\rangle = -k_D(\nabla p)\,\nabla p \tag{34}$$

where $\langle \rho\,\mathbf{u}\rangle$ is the average momentum in the computational domain and can be considered macroscopically as a point value because lattice dimensions are much smaller than electrode thickness. Darcy's law prescribes that the hydraulic parameter can be assumed to be approximately constant.

Here, the flow in a set of randomly generated porous structures was analysed, thus obtaining a distribution of values for Darcy's constant (k_D). A typical example of the considered porous geometry is reported in Figure 2.

FUEL CELL MODEL

In order to evaluate the effect of different resistance constants on a PEM fuel cell performance, a one-dimensional implementation of a fuel cell model was used. Its features are briefly described here.

Fluid flow was modelled using continuity, species conservation, and the Navier-Stokes equations, modified to take into account the porosity of the flow domain, i.e. continuity:

$$\int_\Omega \left[\frac{\partial(\omega\rho)}{\partial t} + \nabla\cdot(\mathrm{K}\,\rho\,\mathbf{u})\right] d\Omega = 0 \tag{35}$$

species conservation:

$$\int_\Omega \left[\frac{\partial(\omega\rho_k)}{\partial t} + \nabla\cdot(\rho_k\,\mathrm{K}\,\mathbf{u}) + -\nabla\cdot(\Gamma_k\,\mathrm{K}\,\nabla\rho_k) - \omega\,S_k\right] d\Omega = 0 \tag{36}$$

and momentum conservation:

$$\int_\Omega \left[\frac{\partial(\omega\rho\,\mathbf{u})}{\partial t} + \nabla\cdot(\rho\,\mathrm{K}\,\mathbf{u}\otimes\mathbf{u}) + + \omega\nabla p - \nabla\cdot(\mathrm{K}\,\mathbf{\Lambda}) - \omega\,S_u\right] d\Omega = 0 \tag{37}$$

The fluid flow was considered isothermal and motion of charges was modelled with Maxwell's fourth equation for charge conservation:

$$\int_\Omega (\nabla^2\varphi - S_\varphi)\,d\Omega = 0 \tag{38}$$

As the characterization of the porous media presented here does not take into account the effect of the presence of liquid water in the electrode pores, the water present in the cell was considered to be in the vapour phase, and the membrane was assumed to be fully humidified. This approach was shown to yield accurate predictions [12], as long as the cell operates in regions of the polarization curve where mass transfer losses, strictly connected with electrode flooding, are negligible.

A single domain approach was followed; i.e. boundary conditions were applied only at the cell boundaries and not at the interface of each single component of the cell (such as electrodes, membrane, catalyst layers and gas channels). As a result, source

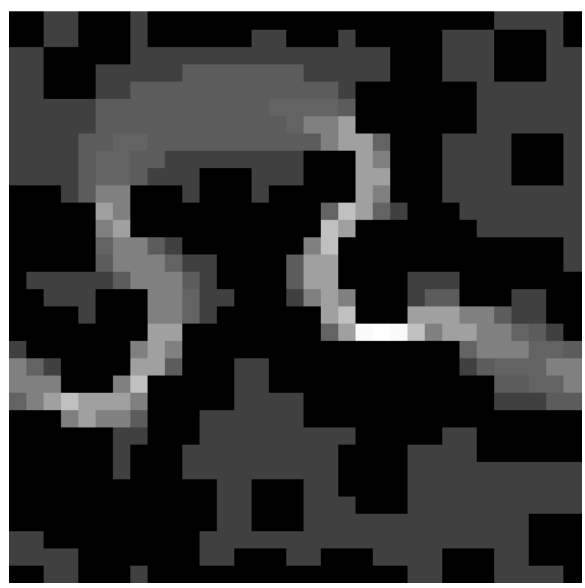

Fig. 2: Example of the porous structure (void fraction 50 %). The black regions are solid obstructions. The fluid regions are marked by grey scale according to velocity magnitude.

terms were added to modify the aforementioned equations to take into account particular phenomena occurring in some of the domain sub-regions. For example, proton production occurs in the anode catalyst layer, hence a sink term

$$S_{H_2} = -\frac{jA_{cell}M_{H_2}}{2FV_{C.L.}} = -\frac{jM_{H_2}}{2FL_{C.L.}} \tag{39}$$

is added to the hydrogen species equation.

Oxygen destruction and water production occur in the cathode catalyst layer, where the terms

$$S_{O_2} = -\frac{jM_{O_2}}{4FL_{C.L.}} \tag{40}$$

$$S_{H_2O} = \frac{jM_{H_2O}}{2FL_{C.L.}} \tag{41}$$

are added.

Source terms in the momentum equation are used to account for additional body forces, namely Darcy's drag and electro-osmotic drag. As a result, the source term becomes

$$S_{u,B.L.} = -R\,\mathbf{u} \tag{42}$$

in the electrode backing layers, and

$$S_{u,C.L.,M.L.} = -R\,\mathbf{u} + \frac{k_\Phi}{k_h} z_f c_f F \nabla\Phi_m \tag{43}$$

in the catalyst layers and membrane.

The source term for the charge conservation equation differs from zero only in the catalyst layers, as charge flows out of the anode, through the electric circuit, and back into the cathode. It can be easily determined, as it is strictly linked to the cell electric current density, i.e.

$$S_\varphi = -\frac{j}{C_m^{eff}} \tag{44}$$

where the membrane conductance varies according to water content and temperature, as found by Springer et. al. [3]

The cell electric potential can be defined as the difference between the maximum (reversible) cell voltage and all the voltage losses inside the cell such that

$$\Phi_{cell} = \Phi_{rev} - \sum \varphi_i \tag{45}$$

where:

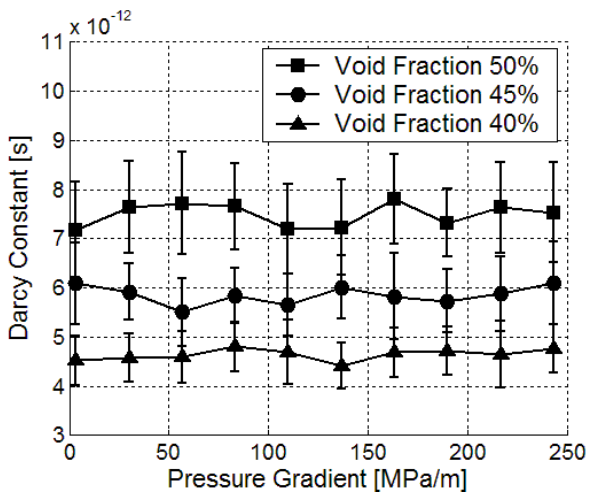

Fig. 3: Calculated values for Darcy's constant (error bars define the range $[\langle k_D\rangle - \sigma, \langle k_D\rangle + \sigma]$)

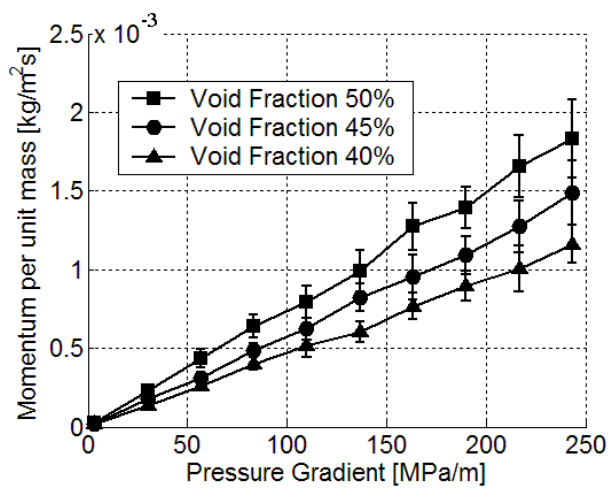

Fig. 4: Calculated mass flow rates (error bars define the range $[\langle k_D\rangle - \sigma, \langle k_D\rangle + \sigma]$)

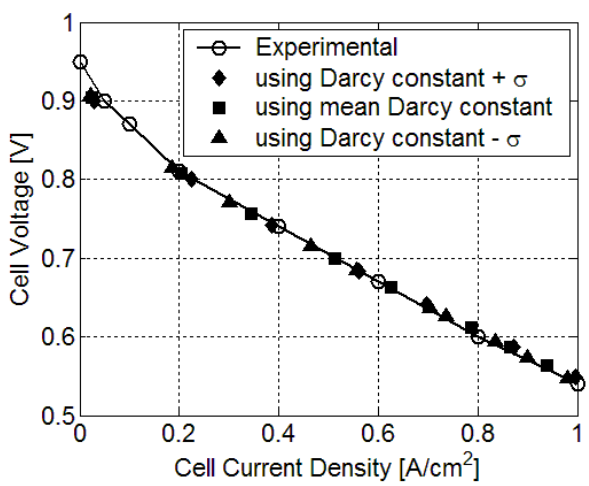

Fig. 5: Effect of Darcy's constant on polarization.

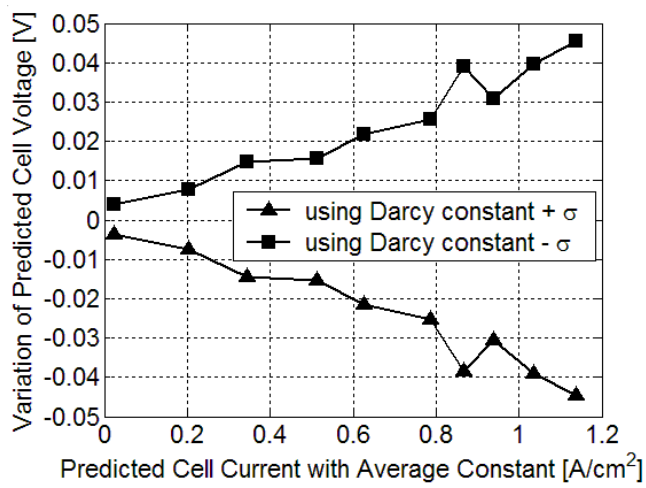

Fig. 6: Effect of Darcy's constant on cell voltage.

$$\Phi_{rev} = \Phi_{rev,0} + \frac{RT}{2F}\left[ln\, p_{H_2} + 0.5\, ln\, p_{O_2} - ln\, p_{H_2O}\right] \quad (46)$$

Reaction activation losses can be represented by an "activation" voltage loss [16]. Reaction kinetics and activation voltage loss are strictly related, as described by the Butler-Volmer equation namely,

$$j = Aj_{ex}\left(\frac{C_k}{C_{k0}}\right)^{\beta_k}\left[e^{\frac{\gamma_a F \varphi_{act}}{RT}} - e^{-\frac{\gamma_c F \varphi_{act}}{RT}}\right] \quad (47)$$

Other losses that need to be taken into account are ohmic losses in the electrodes. Under the hypothesis of homogeneous and isotropic electrode porosity, the electrode conductance can be considered constant, and the ohmic losses can be described by a particular case of Ohm's Law given by the more general equation (38). The ohmic losses are, thus

$$\varphi_\Omega = \frac{I}{C} \quad (48)$$

Combining all the losses, equation (45) becomes:

$$\Phi_{cell} = \Phi_{rev} - \varphi_{act,a} - \varphi_{act,c} - \varphi_{\Omega,c} - \varphi_{\Omega,c} - \varphi_{act,c} \quad (49)$$

To close the model two further equations must be provided. The first one allows the calculation of the nitrogen partial density without solving a transport equation for this species, applying the constraint:

$$\begin{aligned} \rho_{N_2} &= \rho - \rho_{H_2} - \rho_{H_2O} \quad \text{(anode side)} \\ \rho_{N_2} &= \rho - \rho_{O_2} - \rho_{H_2O} \quad \text{(cathode side)} \end{aligned} \quad (50)$$

while the second one allows the correlation of cell voltage and current via the external load connected to the cell stack, providing a feedback relation to equation (45). Thus,

$$j = \frac{\Phi_{stack}}{ZA_{cell}} = \frac{N_{cell}\,\Phi_{cell}}{ZA_{cell}} \quad (51)$$

Finally, Dirichlet boundary conditions for velocity at inlet and pressure at outlets were applied. Inlet gas velocities were calculated according to the stoichiometry of the reactions, using the reference cell current density value of 1.2 A/cm^2.

Neumann no-flux boundary conditions for all the variables were applied elsewhere in the domain.

RESULTS AND DISCUSSION

A two-dimension Lattice Boltzmann model using a nine-velocities computational molecule was used to solve for the flow field in randomly generated porous structures with different porosities. The final purpose was to evaluate the possible dependence of the hydraulic constant upon the porous structure geometry, when varying the macroscopic void fraction and the applied pressure gradient.

The operating conditions of a real fuel cell cathode were used to characterize a physical computational domain, which represents a square two-dimensional portion of porous medium with a 0.8 μm side. Some test configurations were generated by considering different values of porosity (40%, 45% and 50%) and a set of pressure gradients (ten values in the range 3 to 243 MPa/m). The analysis of each configuration was repeated for a statistically significant number (thirty) of porous structures. The related flow field was obtained, thus giving a distribution of hydraulic constants for each porosity value and pressure gradient (figure 3). The mean value of the predicted mass flow rate and the related error bar, were reported in figure 4.

The data obtained from the previous analyses was used in a one dimensional fuel cell model in order to evaluate the effect of

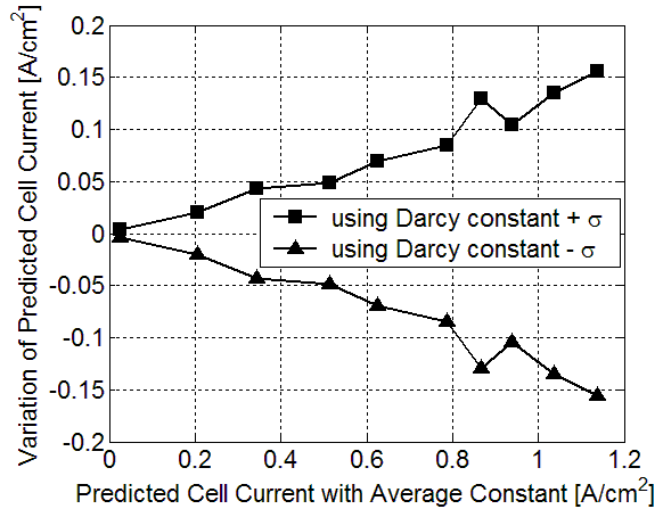

Fig. 7: Effect of Darcy's constant on cell current.

Darcy's constant on the prediction of the cell polarization curve and working point. For each load condition three simulations were carried out, using the mean value of the calculated Darcy constant plus the standard deviation, the mean value, and the mean value minus the standard deviation. Figures 5, 6 and 7 show the results of this analysis for a void fraction of 45 %.

Some interesting conclusions can be drawn from the results obtained in the two analyses. As shown in figure 3, the hydraulic constant was found to vary considerably for different porous materials having the same volume porosity but different distributions of the solid particles in their structure. On the other hand, the second analysis confirmed the suitability of Darcy's law for modelling fluid flow in fuel cell electrodes, as the dependence of velocity on the pressure gradient was found to be linear. However, as figure 4 shows, the dependence of the hydraulic constant on material geometry greatly affects the accuracy of the estimation of the mass flow rate flowing through the porous media for a given pressure gradient in the cell electrode.

As reported in figure 5, the analysis with the fuel cell model showed that a significant variation in the value of Darcy's constant does not affect an accurate prediction of the fuel cell polarization curve.

However, a significant error was found in estimating the exact operating point of the cell as the value of Darcy's constant was varied within the range of twice its standard deviation. Figures 6 and 7 show how the predicted cell current and voltage vary as Darcy's constant varies with respect to its mean value. Voltage differences of 40 to 60 mV were observed. This lack of accuracy can lead to a wrong estimation of cell efficiency, as this is strictly related to the cell voltage [29]. The analysis presented here showed that the different porous structures can lead to errors in efficiency estimation up to 3-5%.

CONCLUSIONS

The present work has dealt with the definition of a procedure for the evaluation of Darcy's constant for porous materials, given their microstructure. Its application to fuel cell electrodes proved to be useful for reducing the uncertainty of estimation of this physical parameter required in fuel cell numerical models. Furthermore, variations in the predicted operating point showed that a parameter usually considered less

significant for cell performance estimation, must indeed be taken with greater care, if greater model accuracy is sought.

The current two-dimensional analysis provided sufficient insight into the problem of material resistance constant estimation. Moreover, work is currently in progress to extend the code to analyse three-dimensional specimens of porous structures, and to simulate the presence of liquid water in the pores. The results that will follow will provide a more accurate estimate of the influence of Darcy's constant on the prediction of fuel cell operation.

The combination of the procedure described here with a tomography scan of the material porous structure could provide a precise, non destructive tool for evaluating material hydraulic characteristics.

ACKNOWLEDGMENTS

The authors would like to acknowledge Prof. Michele Calì for creating the conditions for the development of the present work.

NOMENCLATURE

- a : acceleration due to external field
- A : geometrical area
- B.C. : boundary condition
- C : electric conductance
- c : lattice speed or molar concentration
- D : number of spatial dimensions
- d : diameter
- f : continuous single particle distribution function
- F : Faraday's constant
- I : electric current
- j : electric current density
- K : area porosity
- k : permeability
- L : length
- m : single particle mass
- M : molar mass
- N : number of items
- n : surface normal vector
- p : pressure
- Q : number of discrete microscopic velocities
- R : universal gas constant
- S : source / sink term
- T : temperature
- t : time
- u : macroscopic velocity
- v : microscopic velocity
- V : volume
- Z : load impedance
- z : charge number
- ω : coefficient of quadrature
- Ω : coefficient of quadrature
- β : kinetics exponent
- δ : discrete step
- Γ : diffusion coefficient
- γ : transfer coefficient
- Φ : electric voltage
- ϕ : voltage loss
- Λ : shear stress tensor
- μ : dynamic viscosity
- ρ : density
- σ : standard deviation
- Σ : control volume surface
- τ : collision time
- Ω : control volume
- ω : volume porosity
- ζ : cinematic viscosity

Subscripts and superscripts

- a : anode,
- *B.L.* : backing layer
- *C.L.* : catalyst layer
- *c* : cathode
- *D* : Darcy
- *e* : equilibrium
- *eff* : effective value
- *ex* : exchange
- *flow* : available for fluid flow
- *G.C.* : gas channel
- *h* : hydraulic
- *k* : chemical species
- *M.L.* : membrane layer
- *m* : membrane
- *u* : momentum
- Φ : electrokinetic
- ϕ : related to the charge equation
- *0* : reference value

REFERENCES

[1] Bernardi, D. and Verbrugge, M., 1991,"Mathematical Model of a Gas Electrode Bonded to a Polymer Electrolyte", American Institute of Chemical Engineers Journal, Vol. 37, pp. 1151-1163.

[2] Bernardi, D. and Verbrugge, M., 1992,"A Mathematical Model of the Solid-Polymer-Electrolyte Fuel Cell", Journal of the Electrochemical Society, Vol. 139, pp. 2477-2490.

[3] Springer, T., Zawodinski, T. and Gottesfeld, S., 1991, "Polymer Electrolyte Fuel Cell Model", Journal of the Electrochemical Society, Vol. 138, pp. 2334 -2341.

[4] Springer, T., Wilson, M. and Gottesfeld, S., 1993, "Modeling and Experimental Diagnostics in Polymer Electrolyte Fuel Cells", Journal of the Electrochemical Society, Vol. 140, pp. 3513-3526.

[5] Fuller, T. and Newman, J., 1993, "Water and Thermal Management in Solid-Polymer-Electrolyte Fuel Cells, Journal of the Electrochemical Society, Vol. 140, pp. 1218-1225.

[6] Nguyen, T. and White, R., 1993, "A Water and Heat Management Model for Proton-Exchange-Membrane Fuel Cells", Journal of the Electrochemical Society, Vol. 140, pp. 2178-2186.

[7] Gurau, V., Liu, H. and Kakac, S., 1998, "Two-dimensional Model for Proton Exchange Membrane Fuel Cells", American Institute of Chemical Engineers Journal, Vol. 44, pp. 2410-2422.

[8] Yi, J. and Nguyen, T., 1998, "An Along-the-Channel Model for Proton Exchange Membrane Fuel Cells", Journal of the Electrochemical Society, Vol. 145, pp. 1149-1159.

[9] Yi, J. and Nguyen, T., 1999, "Multi-Component Transport in the Porous Electrodes of PEM Fuel Cells with Interdigitated Gas Distributors,", Journal of the Electrochemical Society, Vol. 146, pp. 38-45.

[10] Gu, W., Wang, Y. and Liaw, B., 1997, "Numerical Modeling of Coupled Electrochemical and Transport Processes in Lead-Acid Batteries," Journal of the Electrochemical Society, Vol.144, pp.2053-2061.

[11] Wang, C., Wang, Z. and Pan, Y.,1999, "Two-phase Transport in Proton Exchange Membrane Fuel Cells", in Proceedings of the International Mechanical Engineering Congress & Exhibits, Nashville, USA.

[12] Um, S., Wang, C. and Chen, K., 2000, "Computational Fluid Dynamics Modeling of Proton Exchange Membrane Fuel Cells", Journal of Electrochemical Society, Vol.147, pp.4485-4493.

[13] Wood, D., Yi, J. and Nguyen, T., 1998, "Effect of Direct Liquid Water Injection and Interdigitated Flow Field on the Performance of

Proton Exchange Membrane Fuel Cells", Electrochimica Acta, Vol. 43, No. 24, pp.3795-3809
[14] Liu, H. and Zhou, T., 2001, "Numerical Simulation of Performance of PEM Fuel Cells", Proceedings of the 2nd International Conference on Computational Heat and Mass Transfer, Rio de Janeiro, Brasil.
[15] Berning, T., Lu, D. and Djilali, N., 2002, "Three-dimensional Computational Analysis of Transport Phenomena in a PEM Fuel Cell", Journal of Power Sources, Vol. 106, p.284-294.
[16] D. H. Rothman, 1988, Geophysics, Vol. 53, p. 509.
[17] J. Bernsdorf, M. Schafer, F. Durst, 1999, International Journal of Numerical Methods in Fluids, Vol. 29, p. 251.
[18] J. Bernsdorf, G. Brenner, F. Durst, 2000, "Numerical analysis of the pressure drop in porous media flow with lattice Boltzmann (BGK) automata", Computer Physics Communications, Vol. 129, p. 246-255.
[19] S. Succi, R. Benzi, F. Higuera, 1991, "The lattice-Boltzmann equation: a new tool for computational fluid dynamics", Lattice Gas Methods: Theory, Applications and Hardware, edited by G. Doolen (Elsevier, Amsterdam), reprinted from Physica D, Vol. 47, p. 219.
[20] S. Chen, G. D. Doolen, 1998, "Lattice Boltzmann method for fluid flow", Annual Review of Fluid Mechanics, Vol. 30, p. 329-338.
[21] C. Cercignani, 1975, "Theory and applications of the Boltzmann equation", Scottish Academic Press, Edinburgh and London, UK.
[22] P. L. Bhatnagar, E. P. Gross, M. Krook, 1954, Physical Review, Vol. 94, p.511.
[23] X. He, X. Shan, G. D. Doolen, 1998, "A discrete Boltzmann equation model for non-ideal gasses", Physical Review E, Vol. 57, R13.
[24] T. Abe, 1997, "Derivation of the lattice Boltzmann method by means of the discrete ordinate method for the Boltzmann equation", Journal of Computational Physics, Vol. 131, p. 241.
[25] Y. H. Qian, D. D'Humieres, P. Lallemand, 1992, "Lattice BGK Models for Navier-Stokes Equations", Europhysics Letters, Vol. 17, p. 479-484.
[26] D. A. Wolf-Gladrow, 2000, "Lattice-gas cellular automata and lattice Boltzmann models: an introduction", Springer, Berlin.
[27] Q. Zou, X. He, 1997, "On pressure and velocity boundary conditions for the lattice Boltzmann BGK model", Physics of Fluids, Vol. 9, p. 1591-1598.
[28] R. S. Maier, R. S. Bernard, D. W. Grunau, 1996, "Boundary conditions for the lattice Boltzmann method", Physics of Fluids, Vol. 8, p. 1788-1801.
[29] Larminie, J. and Dicks, A., 2000, "Fuel Cell Systems Explained" John Wiley and Sons Ltd., ISBN 0-471-49026-1
[30] Ferziger, J. and Peric, M., 1996, "Computational Methods for Fluid Dynamics", Springer-Verlag, ISBN 3-540-59434-5
[31] LeVeque, R., 1990, "Numerical Methods for Conservation Laws", Birkhäuser Verlag, ISBN 0-8176-2464-3